Title

Temperate Earth-sized planets transiting a nearby ultracool dwarf star

Journal

Nature, 533(7602)

ISSN

0028-0836

Authors

Gillon, Michaël
Jehin, Emmanuël
Lederer, Susan M
et al.

Publication Date

2016-05-12

DOI

10.1038/nature17448

Peer reviewed

Published in final edited form as:
Nature. 2016 May 12; 533(7602): 221–224. doi:10.1038/nature17448.

Temperate Earth-sized planets transiting a nearby ultracool dwarf star

Michaël Gillon[1], **Emmanuël Jehin**[1], **Susan M. Lederer**[2], **Laetitia Delrez**[1], **Julien de Wit**[3], **Artem Burdanov**[1], **Valérie Van Grootel**[1], **Adam Burgasser**[4,5], **Amaury H. M. J. Triaud**[6], **Cyrielle Opitom**[1], **Brice-Olivier Demory**[7], **Devendra K. Sahu**[8], **Daniella Bardalez Gagliuffi**[4,5], **Pierre Magain**[1], and **Didier Queloz**[7]

[1]Institut d'Astrophysique et de Géophysique, Université de Liège, Allée du 6 Août 19C, 4000 Liège, Belgium

[2]NASA Johnson Space Center, 2101 NASA Parkway, Houston, Texas, 77058, USA

[3]Department of Earth, Atmospheric and Planetary Sciences, Massachusetts Institute of Technology, 77 Massachusetts Avenue, Cambridge, MA 02139, USA

[4]Center for Astrophysics and Space Science, University of California San Diego, La Jolla, CA, 92093, USA

[5]Visiting Astronomer at the Infrared Telescope Facility, which is operated by the University of Hawaii under Cooperative Agreement no. NNX-08AE38A with the National Aeronautics and Space Administration, Science Mission Directorate, Planetary Astronomy Program

[6]Institute of Astronomy, Madingley Road, Cambridge CB3 0HA, UK

[7]Cavendish Laboratory, J J Thomson Avenue, Cambridge, CB3 0HE, UK

[8]Indian Institute of Astrophysics, Koramangala, Bangalore 560 034, India

Abstract

Stellar-like objects with effective temperatures of 2700K and below are referred to as “ultracool dwarfs”1. This heterogeneous group includes both extremely low-mass stars and brown dwarfs

Correspondence and requests for materials should be addressed to M.G. (michael.gillon@ulg.ac.be).

Author Contributions. The TRAPPIST team (MG, EJ, LD, ArB, CO, PM) discovered the planets. MG leads the exoplanet program of TRAPPIST, set up and organized the ultracool dwarf transit survey, planned and analysed a part of the observations, led their scientific exploitation, and wrote most of the manuscript. EJ manages the maintenance and the operations of the TRAPPIST telescope. SL obtained the DDT time on UKIRT and managed with EJ the preparation of the UKIRT observations. LD and CO scheduled and performed some of the TRAPPIST observations. LD and ArB analysed some photometric observations. JdW led the study of the amenability of the planets for detailed atmospheric characterization. VVG checked physical parameters of the star. AdB checked the spectral type of the star and determined its metallicity. BOD took charge of the dynamical simulations. DBG acquired the SpeX spectra. DS gathered the HCT observations. SL, AT, PM, and DQ assisted writing the manuscript. AT prepared most of the figures in the paper.

Author Information. Reprints and permissions information is available at www.nature.com/reprints. Readers are welcome to comment on the online version of the paper.

The authors declare no competing financial interests.

Online Content. Methods, along with any additional Extended Data display items and Source Data, are available in the online version of the paper; references unique to these sections appear only in the online paper.

Europe PMC Funders Author Manuscripts

(substellar objects not massive enough to sustain hydrogen fusion), and represents about 15% of the stellar-like objects in the vicinity of the Sun2. Based on the small masses and sizes of their protoplanetary disks3,4, core-accretion theory for ultracool dwarfs predicts a large, but heretofore undetected population of close-in terrestrial planets5, ranging from metal-rich Mercury-sized planets6 to more hospitable volatile-rich Earth-sized planets7. Here we report the discovery of three short-period Earth-sized planets transiting an ultracool dwarf star 12 parsecs away using data collected by the TRAPPIST8 telescope as part of an ongoing prototype transit survey9. The inner two planets receive four and two times the irradiation of Earth, respectively, placing them close to the inner edge of the habitable zone of the star10. Eleven orbits remain possible for the third planet based on our data, the most likely resulting in an irradiation significantly smaller than Earth's. The infrared brightness of the host star combined with its Jupiter-like size offer the possibility of thoroughly characterizing the components of this nearby planetary system.

TRAPPIST monitored the brightness of the star TRAPPIST-1 (=2MASS J23062928-0502285) in the very near infrared (~0.9 μm) at high-cadence (~1.2-min) for 245-hours over 62 nights from 17 September to 28 December 2015. The resulting light curves show eleven clear transit-like signatures with amplitudes close to 1% (Extended Data Figs. 1 & 2). Owing to this extensive dataset and to photometric follow-up observations in the visible with the Himalayan Chandra 2m Telescope (India), and in the infrared with the 8m Very Large Telescope (Chile) and the 3.8m UKIRT telescope (Hawaii), nine transits can be attributed to two planets, TRAPPIST-1b and c, transiting the star every 1.51 days and 2.42 days, respectively (Fig. 1 & 2). We attribute the two additional transit signals to a third transiting planet, TRAPPIST-1d, for which 11 orbital periods from 4.5 to 72.8-days are possible based on non-continuous observations (see Table 1). We cannot discard the possibility that the two transits attributed to planet d originate from two different planets, but the consistency of their main parameters (duration, depth, impact parameter) as derived from their individual analyses does not favour this alternative scenario.

TRAPPIST-1 is a well-characterized, isolated M8.0±0.5-type dwarf star11 at a distance of 12.0±0.4 parsecs as measured by its trigonometric parallax12, with an age constrained to be > 500 Myr, and with a luminosity, mass, and radius of 0.05%, 8% and 11.5% those of the Sun13, respectively. We measured its metallicity to be solar based on the analysis of newly acquired infrared spectra. The small size of the host star, only slightly larger than Jupiter, translates into Earth-like radii for the three discovered planets, as deduced from their transit depths. Table 1 presents the physical properties of the system, as derived through a global Bayesian analysis of the transit photometry (Fig. 1) including the *a priori* knowledge of its stellar properties, with an adaptive Markov-Chain Monte Carlo (MCMC) code14.

A non-planetary origin of the transit-like signals is fully discarded by several elements. The first element is the high-proper motion of the star (>1"/yr) that allowed confirmation through archival images that no background source of significant brightness was located behind it in 2015. The second element is the nonexistence of a physical companion of stellar-like nature (star or brown dwarf) around the star, as demonstrated by high-resolution images, radial velocities (RVs), and near-infrared spectroscopy. Together, these two first elements demonstrate that the signals do not originate from eclipses of larger bodies in front of either

a background or physically associated stellar-like object blended with the ultracool target star. They also establish that the light of the target is not diluted by an unresolved additional stellar-like object, validating that the measured transit depths result in terrestrial-sized planetary radii. Other elements include the significant age of the star13, its moderate activity15 and rotation (vsin=6±2 kms^{-1}; P_{rot} = 1.40±0.05 days as measured from our photometry), and its low level of photometric variability16 (confirmed by our data), which are inconsistent with exotic scenarios based on ultra-fast rotation of photospheric structures or occultations by circumstellar material of non-planetary origin (e.g. disk patches, comets)17.

Further confirmations of the planetary origin of the transits come from (1) the periodicity of the transits of planets b and c, and the achromaticity of the transits of planet b as observed from 0.85 μm (HCT) to 2.09 μm (VLT) (Fig. 1.a); and (2) the agreement between the stellar density measured from the transit light curves, $49.3^{+4.1}_{-8.3}\rho_{\odot}$, with the density inferred from the stellar properties, 55.3±12.1 $\rho_{\odot}$.

The masses of the planets and thus their compositions remain unconstrained by these observations. Planetary thermal evolution models and the intense XUV (1-1000Å) emission of low-mass stars18 during their early lives make thick H/He gas envelopes highly unlikely for such small planets19. Statistical analyses of *Kepler* sub-Neptune-sized planets indicate that most Earth-sized planets in close-orbit around solar-type stars are rocky20,21. Still, the paucity of material in the inner region of an ultracool dwarf protoplanetary disk would challenge the *in situ* formation of rocky planets the size of Earth6, favouring thus compositions dominated by ice-rich material originating from beyond the ice line7. The confirmation of this hypothesis will require precise mass measurements to be able to break the degeneracy between the relative amounts of iron, silicates, and ice22. Next-generation high-precision infrared velocimeters should be able to measure the low-amplitude (0.5 to a few $m.s^{-1}$) Doppler signatures of the planets. Alternatively, the planets' masses could be constrained by the transit timing variations (TTVs) caused by their mutual gravitational interactions23, or by transit transmission spectroscopy24.

Given their short orbital distances, it is likely that the planets are tidally locked, i.e. that their rotations have been synchronized with their orbits by tidal interactions with the host star25. Although planets b and c are not in the host star's habitable zone10 (HZ, 0.024 to 0.049 astronomical unit, as defined by 1D models that are not adequate for modeling the highly asymmetric climate of tidally-locked planets26), they have low enough equilibrium temperatures to possibly present habitable regions, in particular, the western terminators of their daysides27 (see Fig. 2 and Table 1). The main concern regarding the localized habitability on tidally-locked planets relates to atmospheric and/or water trapping on their night sides29. Nevertheless, the relatively large equilibrium temperatures of planets b and c would likely prevent such trapping27. In contrast, planet d orbits within or beyond the HZ of the star, its most likely periods corresponding to semi-major axes between 0.033 and 0.093 astronomical units. Unlike the two inner planets, we estimate tidal circularization timescales for planet d to be larger than 1 Gyr. Tidal heating due to a non-zero orbital eccentricity could thus have a significant influence on its global energy budget and its potential habitability28.

The planets' atmospheric properties, and thus their habitabilities, should depend on several unknown factors, notably the planets' compositions, their formation and dynamical (migration, tides) history, the past evolution and current level of the XUV stellar flux29 (probably strong enough in the past, and perharps even now, to significantly alter the planets' atmospheric compositions30), and the past and current amplitudes of atmospheric replenishment mechanisms (impacts, volcanism). Fortunately, the TRAPPIST-1 planets are particularly well-suited for detailed atmospheric characterization, notably by transmission spectroscopy (see Fig. 3), as transit signals are inversely proportional to the square of the host-star radius. Data taken with the *Hubble Space Telescope* (HST) should offer initial constraints on the extent and composition of their atmospheric terminators. The next generation of observatories will allow for a far more in-depth exploration of their atmospheric properties. In particular, data from the *James Webb Space Telescope* (JWST) should yield strong constraints on the atmospheric temperatures and abundances of molecules with large absorption bands, including several biomarkers, like H_2O, CO_2, CH_4, and O_3.

Methods

Spectral type, parallax, and age of the star

TRAPPIST-1 = 2MASS J23062928-0502285 was discovered in 2000 by a search for nearby ultracool dwarfs based on photometric criteria31 and identified as a high proper-motion (μ_α=0.89”, μ_δ=-0.42”), moderately active ($\log L_{H\alpha}/L_{bol}$=-4.61), M7.5 dwarf at ~11 parsecs. Subsequent studies converged to a spectral type of M8.0±0.511,32, while confirming a moderate level of activity typical of similar spectral type stars in the vicinity of the Sun15, 33, 34. The spectral classification was checked by comparing a low-resolution (R~150) near-infrared spectrum of the star13 obtained with the SpeX spectrograph35 mounted on the 3m NASA Infrared Telescope Facility to several spectral type standards, and the best-fit was obtained with the spectrum of the M8-type standard LHS 132 (Extended Data Fig. 3.a). The CTIOPI project reported the star's trigonometric parallax as π=82.6±2.6 mas12, which translates to a distance of 12.1±0.4 parsecs. High-resolution optical spectroscopy failed to detect significant absorption at the 6708 Å Li line36, inferring that the object is not a very young brown dwarf but rather a very-low-mass main-sequence star. This is in agreement with its thick disk kinematics36, its relatively slow rotation (vsini=6±2 $km.s^{-1}$)15, its moderate activity, and its reported photometric stability16 that all point to an age of at least 500 Myrs13.

Metallicity of the star

We obtained new near-infrared (0.9-2.5 μm) spectroscopy of TRAPPIST-1 with the SpeX spectrograph on the night of 2015 November 18 (UT) during clear conditions and 0.8" seeing at K-band. We used the cross-dispersed mode and 0.3"x15" slit aligned at the parallactic angle, to acquire moderate-resolution data ($\lambda/\Delta\lambda \approx 2000$) with dispersion 3.6 Å $pixel^{-1}$ covering the spectral range 0.9-2.5 μm in seven orders. Ten exposures of 300s each were obtained over an airmass range of 1.14-1.17, followed by observations of the A0V star 67 Aqr (V = 6.41) at an airmass of 1.19 for telluric and flux calibration, as well as internal lamp exposures. Data were reduced using the SpeXtool package version 4.0437,38.The

reduced spectrum has a median signal-to-noise of 300 in the 2.17-2.35 μm region, which is shown in Extended Data Fig. 3.b, with metallicity-sensitive NaI (2.206, 2.209 μm) and CaI (2.261, 2.263, 2.266 μm) atomic features labeled. We measured equivalent widths of these features and the H_2O-K2 index defined in Rojas-Ayala et al. (2012)39, and used the mid- and late-M dwarf metallicity calibration of Mann et al. (2014)40 to determine [Fe/H] = 0.04±0.02 (measurement) ±0.07 (systematic) for TRAPPIST-1. The quadratic sum of the two errors resulted in our final measurement [Fe/H] = 0.04±0.08.

Basic parameters of the star

A recent study13 derived a luminosity $L_\star$= 0.000525±0.000036 $L_\odot$ for TRAPPIST-1, using as input data the trigonometric parallax and VRI magnitudes as measured by the CTIOPI project12, 2MASS JHK magnitudes41, WISE W123 magnitudes42, an optical spectrum measured with KPNO/R-C Spec43, and a near-IR spectrum measured by SpeX/Prism. Using this luminosity and the constraint on the age to be >500 Myr as input, the authors of the study13 derived from evolutionary model isochrones and the Stefan-Boltzmann law the following values for the stellar mass, radius, and effective temperature: $M_\star$= 0.082±0.009 $M_\odot$, $R_\star$= 0.116±0.004 $R_\odot$, and T_{eff} = 2557±64K, respectively. To account for the uncertainties coming from the assumptions and details of the evolutionary models, we performed a new determination of these three basic parameters with recent solar metallicity evolutionary model isochrones that consistently couple atmosphere and interior structures44. We obtained $M_\star$= 0.089 $M_\odot$, $R_\star$= 0.112 $R_\odot$, and T_{eff} = 2615K. We then added the difference between the two determinations quadratically to the errors of Filippazzo et al.13, adopting finally $M_\star$= 0.082±0.011 $M_\odot$, $R_\star$= 0.116±0.006 $R_\odot$, and T_{eff} = 2555±85K. The normal distributions corresponding to these values and errors were assumed as prior probability distribution functions in the Bayesian analysis of our photometric data (see below).

Possible binarity of the star

High-resolution imaging from the ground45,46,47 and from space with HST48 discarded the existence of a companion down to an angular distance of 0.1", corresponding to a projected physical distance of 1.2 au at 12 parsecs, in good agreement with the reported stability of the radial velocity of the star at the ~10 ms^{-1} level over a week49 and at the ~150 ms^{-1} level over ~10 weeks50. We performed spectral binary template fitting51 to the IRTF/SpeX spectroscopy, and statistically reject the presence of an L- or T-type brown dwarf companion that would be visible in a blended-light spectrum. TRAPPIST-1 can thus be considered in all probability as an isolated star.

Upper magnitude limits on a background eclipsing binary (BEB)

We measured the J2000 equatorial coordinates of TRAPPIST-1 in the 2015 TRAPPIST images, using 29 stars from the UCAC2 catalog52 and the Pulkovo Observatory Izmccd astrometric software53. We obtained coordinates of RA=23h06m30.34s, DEC=-05d02m36.44s. Due to the high proper motion of TRAPPIST-1 of ~1"/yr, the presence of a possible background object could be assessed by examining this exact position in several previous images taken from the POSS54 (1953) and 2MASS41 (1998) image catalogs. No possible additional source was detected at its position in any of these images.

The faintest stars detected at other positions in the 2MASS images have J-band magnitudes of ~17. We adopt this value as an absolute lower threshold for the J-band magnitude of a background source blended with TRAPPIST-1 in our TRAPPIST 2015 images. TRAPPIST-1 has a J-band magnitude of 11.3542, and the achromaticity of the transits of TRAPPIST-1b as observed from 0.85 to 2.09 μm imposes that, if they originated from a BEB, the latter would have to be a very red object with a spectral type similar to TRAPPIST-1. Combining these two facts, the BEB scenario would require an unphysical eclipse depth >100% in the photometric bands probed by our observations to match the ~0.8% depths measured after dilution by the light of TRAPPIST-1. The BEB scenario is thus firmly discarded.

Photometric observations and analysis

The TRAPPIST8,55 observations in which the transits were detected consisted of 12,295 exposures of 55-s gathered with a thermoelectrically-cooled 2kx2k CCD camera (field of view of 22' x 22', pixel scale of 0.65''). Most of the observations were obtained through an 'I +z' filter having a transmittance >90% from 750 nm to beyond 1100 nm, the red end of the effective bandpass as defined by the spectral response of the CCD. Based on the spectral efficiency model for TRAPPIST and an optical spectrum of a spectroscopic standard M8V star (VB10), we compute an effective wavelength of 885±5 nm for these observations. For the nights of 20 November and 19 December 2015, the target was close to the full Moon and the observations were performed in the Sloan z' filter to minimize the background. After a standard pre-reduction (bias, dark, flat-field correction), the TRAPPIST automatic pipeline extracted the stellar fluxes from the images using the DAOPHOT aperture photometry software56 for eight different apertures. A careful selection of both the photometric aperture size and of stable comparison stars was then manually performed to obtain the most accurate differential light curves of the target.

Photometric follow-up observations were performed with the HAWK-I near-IR imager57 on the ESO 8m Very Large Telescope (Chile), with the HFOSC optical spectro-imager58 on the 2m Himalayan Chandra Telescope (India), and with the WFCAM Wide-Field infrared CAMera59 located at the prime focus of the 3.8m UKIRT telescope (Hawaii).

The VLT/HAWK-I observations of a transit of planet b were performed during the night of 8 November 2015. HAWK-I is composed of four Hawaii 2RG 2048 x 2048 pixels detectors (pixel scale = 0.106''). Its total field of view on the sky is 7.5'x7.5'. The transit was observed through the narrowband filter NB2090 (λ=2.095μm, width=0.020μm). 185 exposures composed of 17 integrations of 1.7s each were acquired during the run in stare mode, i.e. without applying a jitter pattern. After standard calibration of the images, stellar flux measurement was performed by aperture photometry14.

The HCT/HFOSC observations of a transit of TRAPPIST-1b were performed on 18 November 2015. The imager in the HFOSC CCD detector is an array of 2048x2048 pixels corresponding to a field of view of 10'x10' on-sky (pixel scale=0.3''). The observations consisted of 104 exposures, each 20-s taken in stare mode and in the I filter, centered on the expected transit time. After a standard calibration of these images and their photometric reduction with DAOPHOT, differential photometry was performed. We estimate the effective

wavelength of these observations to be 840±20 nm, based on the spectral response of HFOSC and an optical spectrum of the M8V standard star VB10.

The UKIRT/WFCAM observations of 2 transits of planet b and 1 transit of planet c consisted of 3 runs of 4 hrs each, performed on 5, 6 and 8 December 2015 in J-band. WFCAM is composed of four HgCdTe detectors of 2048x2048 pixels each, with a pixel scale of 0.4" resulting in a field of view of 13.65'x13.65' for each detector. On 5 December 2015, 1365 exposures composed of 3 integrations of 2s each were performed in stare mode. For the runs on 6 and 8 December 2015, respectively, 1181 and 1142 exposures composed of five 1s-exposures were performed, again in stare mode and using the same pointing as 5 Dec 2015. Differential aperture photometry was performed with DAOPHOT on all calibrated images.

Global analysis of the photometry

We inferred the parameters of the three detected planets transiting TRAPPIST-1 from the analysis of their transit light curves (Extended Data Fig. 1 and Extended Data Table 1) with an adaptive Markov-Chain Monte Carlo (MCMC) code14. We converted each UT time of mid-exposure to the BJD_{TDB} time system60. The model assumed for each light curve was composed of the eclipse model of Mandel & Agol (2002)61 multiplied by a baseline model aiming to represent the other astrophysical and instrumental mechanisms able to produce photometric variations. Assuming the same baseline model for all light curves, and minimizing the Bayesian Information Criterion (BIC)62, we selected a second-order time polynomial as a baseline model to represent the curvature of the light curves due to the differential extinction and the low-frequency variability of the star, and added an instrumental model composed of a second-order polynomial function of the positions and widths of the stellar images.

Stellar metallicity, effective temperature, mass, and radius were four free parameters in the MCMC for which prior probability distribution functions (PDFs) were selected as input. Here, the normal distributions $\mathcal{N}(0.04, 0.08^2)$ dex, $\mathcal{N}(2555, 85^2)$ K, $\mathcal{N}(0.082, 0.011^2)$ $M_\odot$, and $\mathcal{N}(0.114, 0.006^2)$ $R_\odot$ were assumed based on *a priori* knowledge of the stellar properties (see Basic parameters of the star). Circular orbits were assumed for all transiting objects. For each of them, the additional free parameters in the MCMC included (1) the transit depth dF defined as $(R_p/R_\star)^2$, with R_p and $R_\star$ the planetary and stellar radii, respectively (2) the transit impact parameter $b = a\cos i/R_\star$, with a and i the planet's semi-major axis and orbital inclination, respectively (3) the orbital period P, (4) the transit width W defined as $(P R_\star/a)[(1+R_p/R_\star)^2 - b^2]^{1/2}/\pi$, and (5) the mid-transit time (time of inferior conjunction) T_0. Uniform prior distributions were assumed for each of these free parameters. At each step of the MCMC, values for R_p, a, i, were computed from the values for the transit and stellar parameters, as well as values for the irradiation of the planet in Earth units and for its equilibrium temperatures assuming a Bond albedo of 0 and 0.75, respectively. A quadratic limb-darkening law62 was assumed for the star. For each bandpass, values and errors for the limb-darkening coefficients u_1 and u_2 were derived from the Claret & Bloemen tables (2011)63 (see Extended Data Table 2), and the corresponding normal distributions were used

as prior PDFs in the MCMC. u_1 and u_2 were free parameters under the control of these PDFs in the MCMC.

We divided our analysis into three phases. The first phase focused on the two inner planets, for which the period is firmly determined. A circular orbit was assumed for both planets. All transit light curves of the two planets were used as input data for this first phase, except the TRAPPIST light curve of 11 December 2015 for which the transit of planet c is blended with a transit of planet d. A preliminary MCMC analysis composed of 1 chain of 50,000 steps was first performed to estimate the need to rescale the photometric errors14. Then a longer MCMC analysis was performed, composed of 5 chains of 100,000 steps whose convergence was checked using the statistical test of Gelman & Rubin64. The parameters derived from this analysis for the star and its two inner planets are shown in Table 1. We performed a similar analysis assuming a uniform prior PDF for the stellar radius to derive the value of the stellar density constrained only by the transit photometry65. It resulted in a stellar density of $49.3^{+4.1}_{-8.3}\rho_{\odot}$, in excellent agreement with the density of 55.3±12.1 $\rho_{\odot}$ derived from the *a priori* knowledge of the star, bringing thus a further validation of the planetary origin of the transit signals.

In the second phase of our analysis, we performed 11 global MCMC analyses of all transit light curves, each of them consisting of one chain of 50,000 steps and corresponding to one of the possible values of the period of TRAPPIST-1d (see Table 1) for which a circular orbit was assumed. We then repeated the 11 analyses under the assumption of an eccentric orbit for planet d. We used the medians of the BIC posterior distributions to compare the relative posterior probability of each orbital model through the formula $P1/P2=e^{(BIC_2-BIC_1)/2}$. The resulting relative probabilities are given in Extended Data Table 3. It shows that our data favour (relative probability > 10%) a circular orbit and an orbital period between 10.4 and 36.4 days, the most likely period being 18.4 days.

In the final phase, we performed individual analyses of the light curves to measure the mid-eclipse time of each transit to support future TTV studies of the system22, 66. The resulting timings are shown in Extended Data Table 4. They do not reveal any significant TTV signal, which is not surprising given the amplitude of the expected periodicity departures (see below) combined with the limited timing precision of the TRAPPIST photometry.

Extended Data Fig. 1 and 2 show the raw and detrended light curves, respectively, and for each of these the best-fit eclipse + baseline model is overplotted in the figures. The phased-time detrended light curves are shown for each planet and bandpass in Fig. 1.

Photometric variability of the star

The TRAPPIST dataset was used to assess the photometric variability of the star at ~900 nm. On the timescale of a few hours, corresponding to the typical duration of our observing runs, the star appears to be relatively stable, except for the transits and for 4 sharp, low-amplitude (1 to a few %) increases of brightness followed by exponential-type decreases to the normal levels within 10-15 minutes (Extended Data Fig. 4) that we attribute to flares67. The low amplitude and inferred low frequency (1/60 hr^{-1}) of these flares is consistent with

the reported low level of activity of the star15,33,34, strengthening the inference that the system is not young.

To assess the lower-frequency variability of TRAPPIST-1, we built its global differential light curve in the I+z filter, using four stable stars of similar brightness in the TRAPPIST images as comparison stars. We filtered out the flares, transits, and measurements taken in cloudy conditions to create the resulting light curve consisting of 12,081 photometric measurements. It is compared to the light curve for the comparison star 2MASSJ23063445-0507511 in Extended Data Fig. 5.a. It clearly shows some variability at the few % level, which is consistent with previous photometric results obtained in the I-band16. A Lomb-Scargle (LS) periodogram68 analysis of the light curve, filtered out of low-frequency variations and differential extinction by division of the best-fit 4th-order polynomial in time and airmass, reveals a power excess with a period of 1.4 days (see Extended Data Fig. 5.b). Cutting the light curves in two, and in four in a second test, and performing a LS analysis of each fraction, revealed a power excess at ~1.4 days for all of them, supporting a genuine periodic signal of astrophysical origin. Associating it with the stellar rotation period, the resulting equatorial rotation speed of 4.1 km.s^{-1} (assuming $R_{\star}$= 0.114 $R_{\odot}$) is consistent with the literature measurement15 vsini=6±2 km.s^{-1}, making this association physically meaningful. Based on the scatter of the peak values obtained in the LS analyses of the light curve fractions, we estimate the error bar on the rotation period of 1.40 days to be 0.05 day. In summary, the photometric variability of the star appears thus to be dominated by the rotation and evolution of photospheric inhomogeneities (spots) combined with rare flares.

Dynamics of the system

We computed the tidal circularization timescales69 $t_{circ}=\frac{2PQ}{63\pi}\times\frac{M_p}{M_*}\times\left(\frac{a}{R_p}\right)^5$ of the three planets, assuming planetary masses M_p ranging from 0.45 Earth masses (pure ice composition) to 3 Earth masses (pure iron composition)22 and a tidal quality factor70 Q of 100, corresponding to the maximum value derived for terrestrial planets and satellites of the solar system70. For planets b and c, the computed values range from 22 Myr to 145 Myr and from 177 Myr to 1.1 Gyr, respectively. Taking into account that the system is apparently not very young and that the orbits have weak mutual perturbations as they are not close to any mean-motion resonance, our assumption of circular orbits for the two inner planets is thus reasonable. On the other hand, the same computations result in values ranging from a few to tens of Gyr for planet d, making a significant orbital eccentricity possible from a tidal theory perspective. Still, a nearly-circular orbit for this outer planet is still a reasonable hypothesis when considering the strong anticorrelation of orbital eccentricity and multiplicity of planets detected by radial velocities71, and is favoured by our global analysis of the transit photometry (see above).

We used the Mercury software package72 to assess the dynamical stability of the system over 10,000 years for all possible periods of planet d. Instabilities appeared in our simulations only for the unlikely scenarios of planet d on a significantly eccentric (e≥0.4) 4.5 or 5.2-day orbit.

To assess the potential of the TTV method24, 66 to measure the masses of the planets, we integrated the dynamical evolution of the system at high sampling over 2 years, assuming Earth-masses for the three planets and an 18.4 day circular orbit for TRAPPIST-1d. These simulations resulted in TTV amplitudes of several tens of seconds and led us to conclude that with an intensive transit monitoring campaign with instruments able to reach timing precisions of a few tens of seconds (e.g. VLT/HAWK-I, UKIRT/WFCAM, see Extended Table 4), it should be possible to constrain the planetary masses.

Estimation of the suitability of the planets for detailed atmospheric characterization

We estimated the typical signal amplitude in transit transmission spectroscopy for all the transiting exoplanets with a size equal to or smaller than the mini-Neptune GJ1214b73. We computed it as $2R_p h_{eff}/R_*^2$ where R_p is the planetary radius, h_{eff} the effective atmospheric height (i.e., the extent of the atmospheric annulus), and R_* is the stellar radius. The effective atmospheric height is directly proportional to the atmospheric scale height, H=kT/(μg) where k is Boltzmann's constant, T the atmospheric temperature, μ the atmospheric mean molecular mass, and g the surface gravity. The ratio h_{eff}/H for a clear atmosphere24,74 is typically between 6 and 10 and is thus strongly dependent on the presence of clouds and the spectral resolution and range covered. Our estimates, presented in Fig. 2, are based on an h_{eff}/H ratio of 7 and the conservative assumption of a volatile-dominated atmosphere (μ =20) with a Bond albedo of 0.3. All other parameters for the planets were derived from exoplanets.org75. As illustration, the maximum transit depth variations projected under those assumptions for GJ1214b are of ~250 ppm, in agreement with independent simulations76.

We also derived for the same planets sample typical SNRs in transit transmission spectroscopy from the ratio of our computed signal amplitudes over the square root of the flux (determined from the J-band magnitudes of the host stars). The SNRs of TRAPPIST-1's planets in transmission are expected to range between 0.22 and 0.55 times GJ 1214b's, implying that these planets are well-suited for atmospheric studies with HST/WFC3 similar to those previously targeting GJ1214b76,77.

Based on literature simulations for terrestrial planets24, we estimated that the characterization of planets b, c, and d should require up to 70, 90, and 270 hrs of in-transit observations with JWST, respectively, and yield the atmospheric temperatures with relative uncertainties below 15% and the abundances within a factor of 4. Assuming the atmospheres of TRAPPIST-1's planets are not depleted and do not harbor a high-altitude cloud deck, JWST should notably yield constraints on the abundances of molecules with large absorption bands such as H_2O, CO_2, CH_4, CO, and O_3 if their abundances are ≥10-ppm level.

We also assessed the potential of the cross-correlation technique78 to constrain the atmospheric properties of the TRAPPIST-1 planets, following a literature formalism79. We inferred that detecting O_2 in TRAPPIST-1's planets would require up to 80 transit observations with one of the next generation giant ground-based telescopes. Taking in

account the limited fraction of transits visible at low airmass, such an endeavor could be reached in 5 to 15 years.

Code availability

Equivalent widths and H_2O-K2 index measurements in the SpeX spectra were made using the IDL program created by A. Mann and distributed at http://github.com/awmann/metal. The conversion of the UT times of the photometric measurements to the BJD_{TDB} system was performed using the online program created by J. Eastman and distributed at http://astroutils.astronomy.ohio-state.edu/time/utc2bjd.html. IRAF is distributed by the National Optical Astronomy Observatory, which is operated by the Association of Universities for Research in Astronomy, Inc., under cooperative agreement with the National Science Foundation. The MCMC software used to analyse the photometric data is a custom Fortran 90 code that can be obtained upon request to the first author.

Europe PMC Funders Author Manuscripts

Europe PMC Funders Author Manuscripts

Extended Data

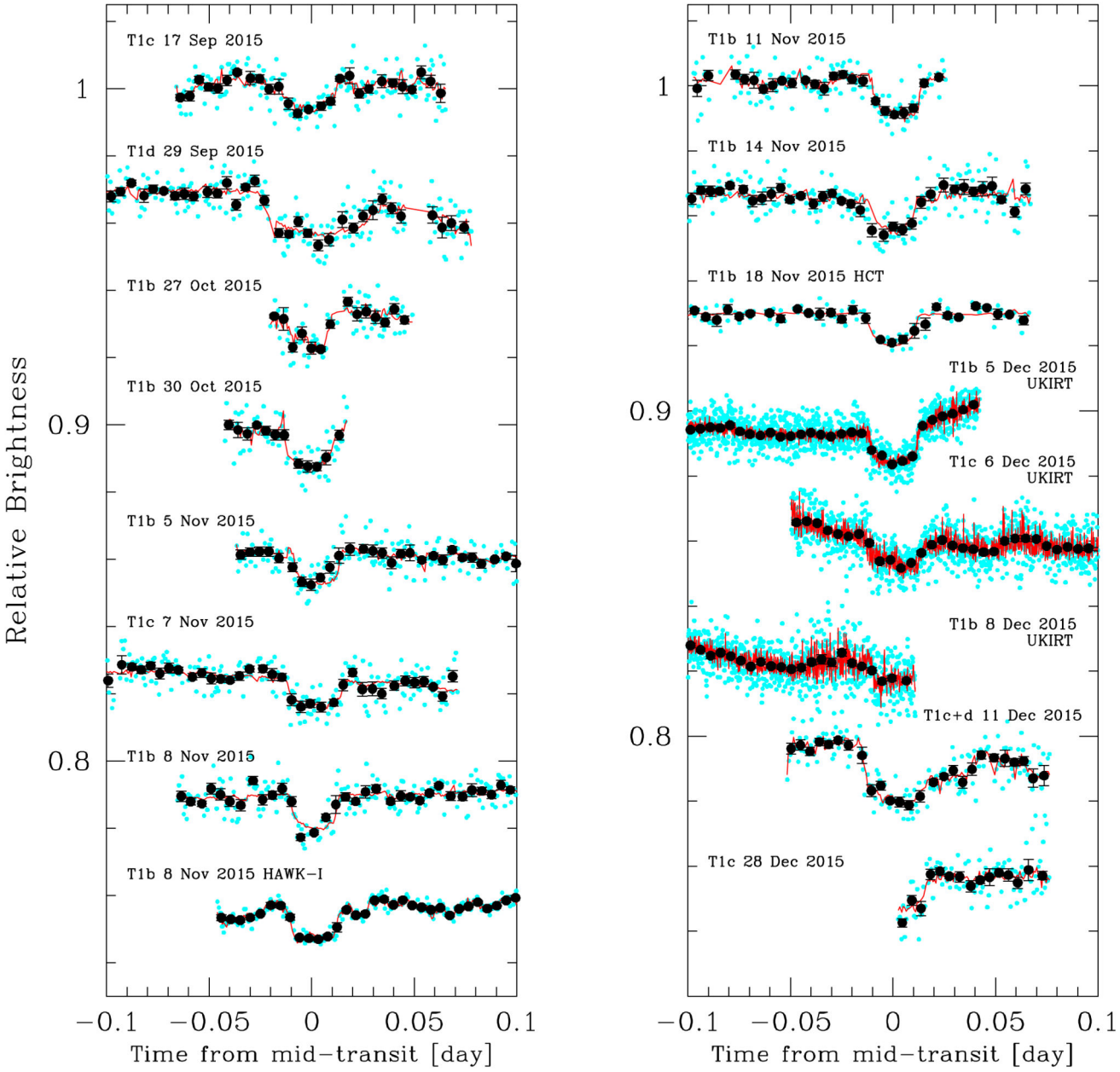

Extended Data Figure 1. Raw TRAPPIST-1 transit light curves.

The light curves are shown in chronological order from top to bottom and left to right, with unbinned (cyan dots) and binned per 0.005-d (7.2-min) intervals (black dots with error bars). The error bars are the standard errors of the mean of the measurements in the bins. The best-fit transit+baseline models are overplotted (red line). The light curves are phased for the mid-transit time and shifted along the *y*-axis for the sake of clarity. For the dual transit of 11 Dec 2015, the light curve is phased for the mid-transit time of planet c.

Europe PMC Funders Author Manuscripts

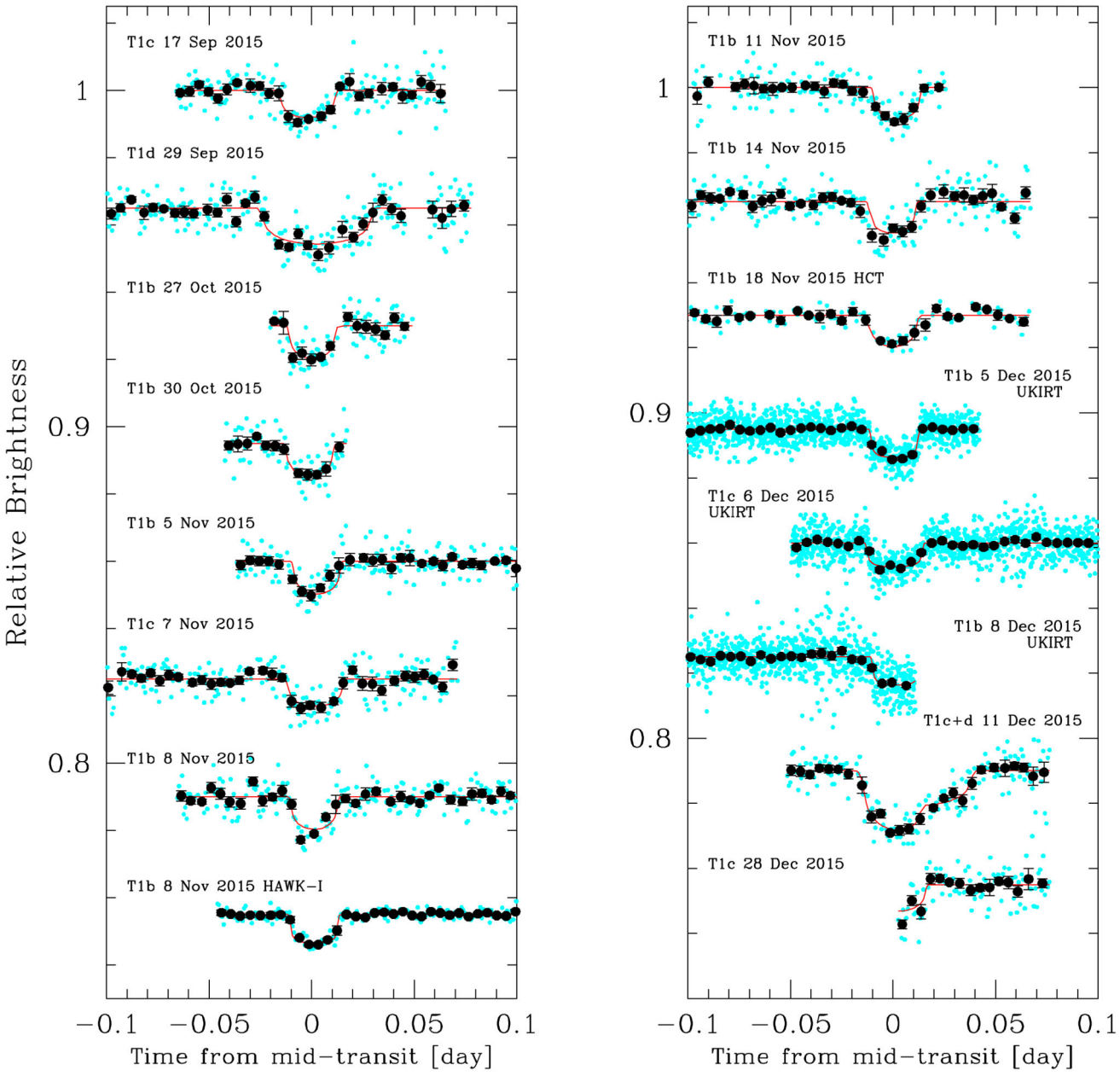

Extended Data Figure 2. Detrended TRAPPIST-1 transit light curves.

Same as Extended Data Fig. 1, except that the light curves are here divided by the best-fit baseline model to highlight the transit signatures.

Europe PMC Funders Author Manuscripts

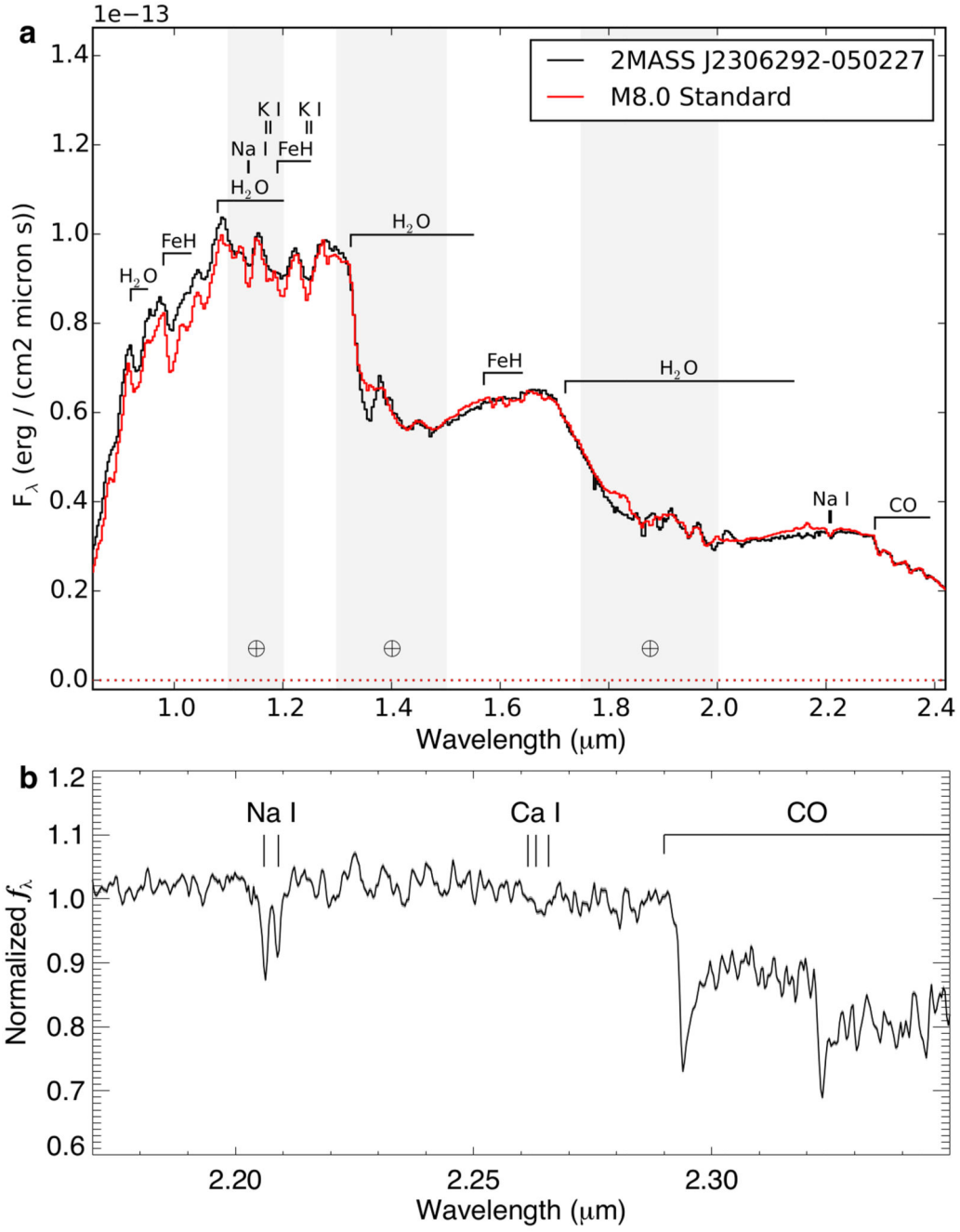

Extended Data Figure 3. Near-infrared spectra of TRAPPIST-1.

a, Comparison of TRAPPIST-1's near-infrared spectrum obtained with the spectrograph IRTF/SpeX35 and the spectrum of the M8-type standard LHS132 (red). **b**, Cross-dispersed IRTF/SpeX spectrum of TRAPPIST-1 in the 2.17-2.35 μm region. NaI, CaI and CO features are labeled. Additional structure is primarily from overlapping H_2O bands. The spectrum is normalized at 2.2 μm.

Europe PMC Funders Author Manuscripts

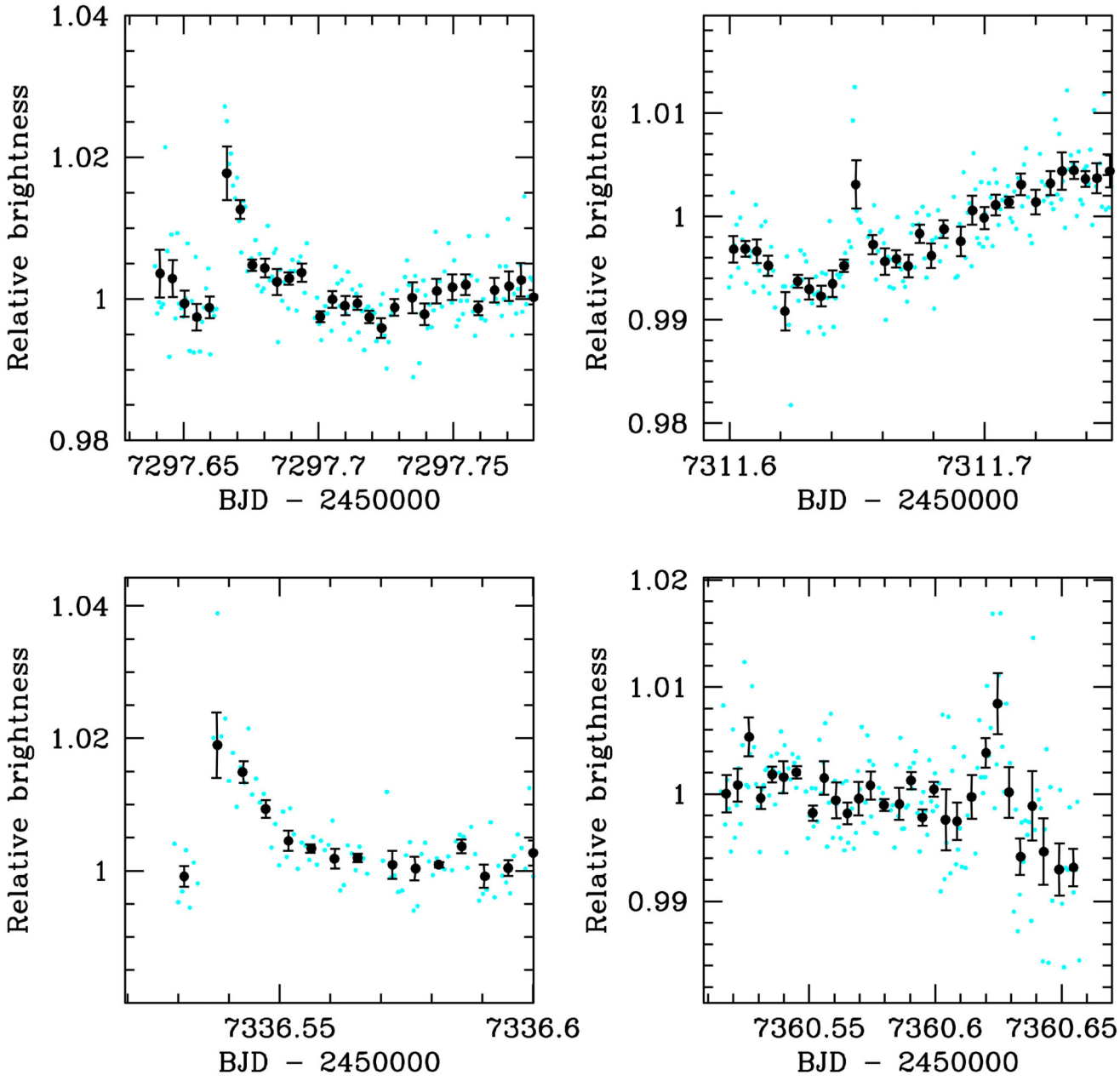

Extended Data Figure 4. Flare events in the TRAPPIST 2015 photometry.

The photometric measurements are shown unbinned (cyan dots) and binned per 7.2-minute intervals. For each interval, the error bars are the standard error of the mean.

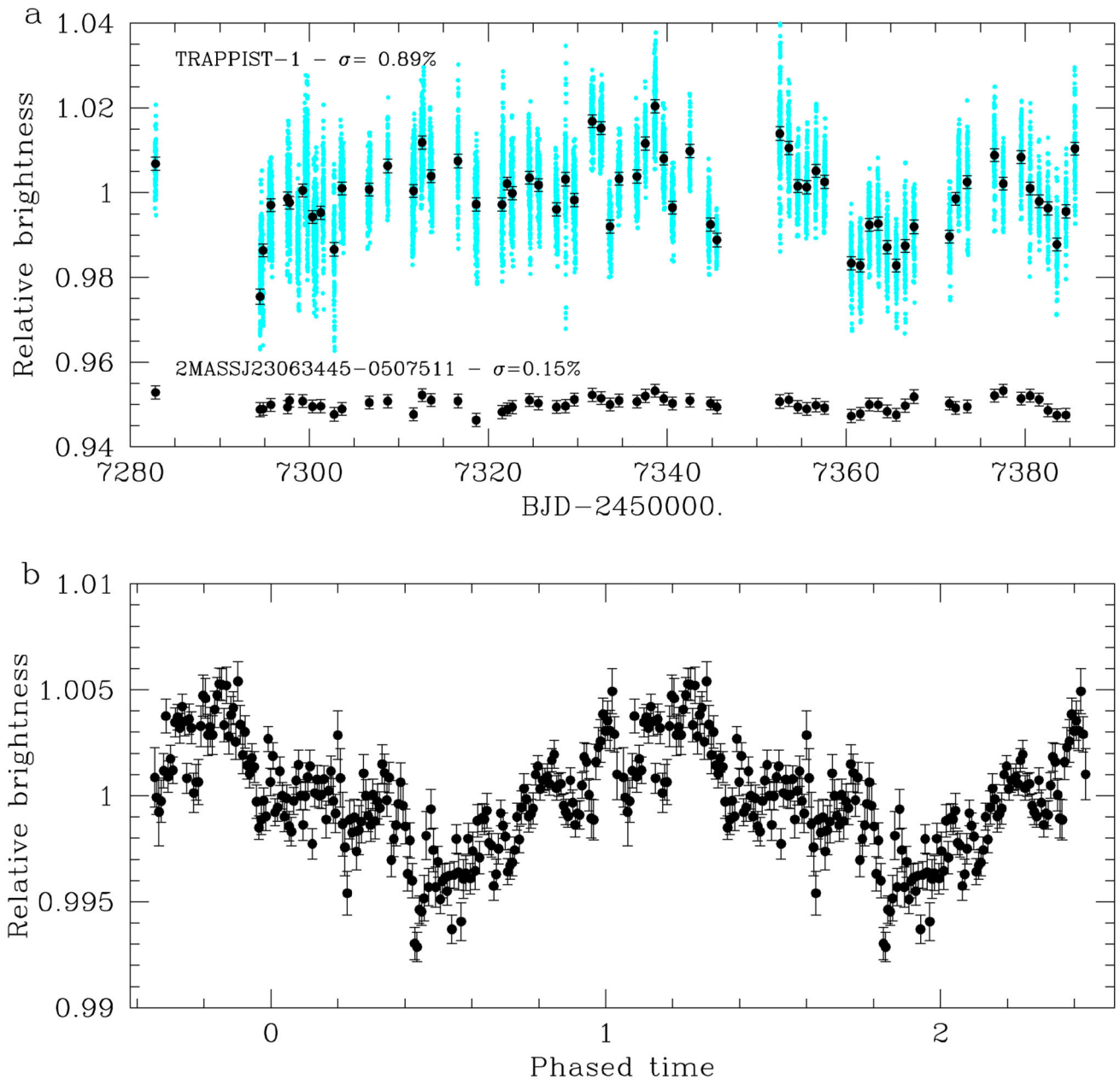

Extended Data Figure 5. Photometric variability of TRAPPIST-1.

a, Global light curve of the star as measured by TRAPPIST. The photometric measurements are shown unbinned (cyan dots) and binned per night (black dots with error bars = standard errors of the mean). It is compared to the light curve of the comparison star 2MASSJ23063445-0507511, shifted along the y-axis for the sake of clarity. **b**, Same light curve folded on the period P=1.40-days and binned by 10-minute intervals (error bars = standard errors of the mean). Two periods are shown in the figure for the sake of clarity.

Europe PMC Funders Author Manuscripts

Extended Data Table 1
TRAPPIST-1 transit light curves.

For each light curve, the instrument, filter, number of points N_p, exposure time T_{exp}, and baseline function are given. For the baseline functions, $p(\varrho^2$ denotes, respectively, a 2nd-order polynomial function of time (ϱ = t), x and y positions (ϱ = xy), and full-width at half-maximum of the stellar images (ϱ = f).

Date	Instrument	Filter	N_p	T_{exp}	Baseline function	Transit(s)
17 Sep 2015	TRAPPIST	I+z	163	55s	$p(t^2+xy^2+f^2)$	TRAPPIST-1c
29 Sep 2015	TRAPPIST	I+z	232	55s	$p(t^2+xy^2+f^2)$	TRAPPIST-1d
27 Oct 2015	TRAPPIST	I+z	84	55s	$p(t^2+xy^2+f^2)$	TRAPPIST-1b
30 Oct 2015	TRAPPIST	I+z	77	55s	$p(t^2+xy^2+f^2)$	TRAPPIST-1b
05 Nov 2015	TRAPPIST	I+z	237	55s	$p(t^2+xy^2+f^2)$	TRAPPIST-1b
07 Nov 2015	TRAPPIST	I+z	241	55s	$p(t^2+xy^2+f^2)$	TRAPPIST-1c
08 Nov 2015	TRAPPIST	I+z	231	55s	$p(t^2+xy^2+f^2)$	TRAPPIST-1b
	VLT/HAWK-I	NB2090	207	17x1.7s	$p(t^2+xy^2+f^2)$	TRAPPIST-1b
11 Nov 2015	TRAPPIST	I+z	140	55s	$p(t^2+xy^2+f^2)$	TRAPPIST-1b
14 Nov 2015	TRAPPIST	I+z	241	55s	$p(t^2+xy^2+f^2)$	TRAPPIST-1b
18 Nov 2015	HCT/HFOSC	I	103	20s	$p(t^2+xy^2+f^2)$	TRAPPIST-1b
05 Dec 2015	UKIRT	J	1312	3x2s	$p(t^2+xy^2+f^2)$	TRAPPIST-1b
06 Dec 2015	UKIRT	J	1175	5x1s	$p(t^2+xy^2+f^2)$	TRAPPIST-1c
08 Dec 2015	UKIRT	J	1109	5x1s	$p(t^2+xy^2+f^2)$	TRAPPIST-1b
11 Dec 2015	TRAPPIST	I+z	158	55s	$p(t^2+xy^2+f^2)$	TRAPPIST-1c + d
28 Dec 2015	TRAPPIST	I+z	94	55s	$p(t^2+xy^2+f^2)$	TRAPPIST-1c (partial)

Extended Data Table 2
Quadratic limb-darkening coefficients.

These values and errors for the quadratic coefficients u_1 and u_2 were inferred for TRAPPIST-1 from theoretical tables63, and used as a priori knowledge of the stellar limb-darkening in the global MCMC analysis of the transit light curves. The error bars were obtained by propagation of the errors on the stellar gravity, metallicity, and effective temperature.

Bandpass	u_1	u_2
I (HCT/HFOSC)	0.72±0.10	0.15±0.11
I+z (TRAPPIST)	0.65±0.10	0.28±0.12
J (UKIRT/WFCAM)	0.10±0.05	0.57±0.02
NB2090 (VLT/HAWKI)	0.04±0.03	0.50±0.03

Extended Data Table 3

Posterior likelihoods of the orbital solutions for TRAPPIST-1d.

The likelihoods shown are normalized to the most likely solution (circular orbit - P=18.204-d). For each orbit, the semi-major axis *a* is given in astronomical units (au), assuming a stellar mass of 0.08 $M_{\odot}$ (Table 1), and the mean irradiation, S_p, in Earth units, S_{Earth}.

TRAPPIST-1d period (d)	Circular orbit	Eccentric orbit	*a* (au)	S_p (S_{Earth})
4.551	0.0016	0.0017	0.023	0.98
5.200	0.0041	0.0045	0.025	0.82
8.090	0.012	0.013	0.034	0.45
9.101	0.018	0.011	0.037	0.39
10.401	0.139	0.0067	0.040	0.33
12.135	0.243	0.0029	0.045	0.26
14.561	0.393	0.0023	0.050	0.21
18.204	1	0.0018	0.058	0.15
24.270	0.212	0.0016	0.071	0.11
36.408	0.122	0.0014	0.093	0.06
72.820	$7.5e^{-5}$	$6.8e^{-8}$	0.147	0.02

Extended Data Table 4

Individual timings measured for the TRAPPIST-1 planets.

The transit timings shown were deduced from individual analyses of the transit light curves, assuming circular orbits for the planets. The error bars correspond to the 1-sigma limits of the posterior PDFs of the transit timings.

Planet	Instrument	Epoch	Mid-transit timing (BJD_{TDB}-2,450,000)
TRAPPIST-1b	TRAPPIST	0	$7322.5161^{+0.0013}_{-0.0010}$
	TRAPPIST	2	$7325.5391^{+0.0035}_{-0.0013}$
	TRAPPIST	6	7331.5803±0.0013
	TRAPPIST	8	7334.6038±0.0012
	VLT/HAWK-I	8	7334.60490±0.00020
	TRAPPIST	10	7337.6249±0.0010
	TRAPPIST	12	$7340.6474^{+0.0010}_{-0.0022}$
	HCT/HFOSC	15	7345.18011±0.00089
	UKIRT/WFCAM	26	7361.79960±0.00030
	UKIRT/WFCAM	28	7364.82137±0.00056
TRAPPIST-1c	TRAPPIST	0	7282.8058±0.0010

Planet	Instrument	Epoch	Mid-transit timing (BJD_{TDB}-2,450,000)
	TRAPPIST	21	7333.6633±0.0010
	UKIRT/WFCAM	33	7362.72623±0.00040
	TRAPPIST	35	7367.5699±0.0012
	TRAPPIST	42	7384.5230±0.0011
TRAPPIST-1d	TRAPPIST	0	7294.7736±0.0014
	TRAPPIST	?	7367. 5818±0.0015

Acknowledgments

TRAPPIST is a project funded by the Belgian F.R.S.-FNRS under grant FRFC 2.5.594.09.F, with the participation of the Swiss FNS. The research leading to these results has received funding from the European Research Council under the FP/2007-2013 ERC Grant Agreement n° 336480, and from the ARC grant for Concerted Research Actions, financed by the Wallonia-Brussels Federation. The material presented here is based on work supported in part by NASA under Contract No. NNX15AI75G. UKIRT is supported by NASA and operated under an agreement among the University of Hawaii, the University of Arizona, and Lockheed Martin Advanced Technology Center; operations are enabled through the cooperation of the East Asian Observatory. The facilites at IAO and CREST are operated by the Indian Institute of Astrophysics, Bangalore, India. M. Gillon, E. Jehin, and V. Van Grootel are F.R.S.-FNRS Research Associates. L. Delrez and C. Opitom are F.R.S.-FNRS PhD students. The authors thank V. Mégevand, the ASTELCO team, and S. Sohy for their contribution to the TRAPPIST project; the Liverpool Telescope team, Ö. Baştürk, and M. Bretton for their attempts to measure the transits; the IRTF operators B. Cabreira and D. Griep for their assistance with the SpeX observations; the UKIRT staff scientists W. Varricatt & T. Kerr, telescope operators S. Benigni, E. Moore, and T. Carroll, and CASU scientists G. Madsen and M. Irwin for their assistance with the UKIRT observations; the ESO astronomers A. Smette & G. Hau for their diligent efforts to provide us with the best possible VLT data; the staff of IAO, Hanle and CREST, Hosakote, that made observations with HCT possible.

References

1. Kirkpatrick JD, Henry TJ, Simon DA. The solar neighborhood. 2: the first list of dwarfs with spectral types of M7 and cooler. Astron J. 1995; 109:797–807.
2. Cantrell JR, Henry TJ, White RJ. The solar neighborhood XXIX: the habitable real estate of our nearest stellar neighbours. Astron J. 2013; 146:99.
3. Andrews SM, Wilner DJ, Hugues AM, Qi C, Dullemond CP. Protoplanetary disk structures in Opiuchus. II. Extension to fainter sources. Astrophys J. 2010; 723:1241–1254.
4. Lyu Y, Joergens V, Bayo A, Nielbock M, Wang H. A homogeneous analysis of disk around brown dwarfs. Astron & Astrophys. 2015; 582:A22.
5. Payne MJ, Lodato G. The potential for Earth-mass planet formation around brown dwarfs. Mon Not R Astron Soc. 2007; 381:1597–1606.
6. Raymond SN, Scalo J, Meadows VS. A decreased probability of habitable planets formation around low-mass stars. Astrophys J. 2007; 669:606–614.
7. Montgomery R, Laughlin G. Formation and detection of Earth-mass planets around low mass stars. Icar. 2009; 202:1–11.
8. Gillon M, et al. TRAPPIST: a robotic telescope dedicated to the study of planetary systems. EPJ Web Conf. 2011; 11:06002. http://www.epj-conferences.org/articles/epjconf/abs/2011/01/epjconf_ohp2010_06002/epjconf_ohp2010_06002.html.
9. Gillon M, Jehin E, Fumel A, Magain P, Queloz D. TRAPPIST-UCDTS: a prototype search for habitable planets transiting ultra-cool stars. EPJ Web Conf. 2013; 47:03001. http://www.epj-conferences.org/articles/epjconf/abs/2013/08/epjconf_hpcs2012_03001/epjconf_hpcs2012_03001.html.
10. Kopparapu RK, et al. Habitable zones around main-sequence stars: new estimates. Astrophys J. 2013; 765:131.

11. Liebert J, Gizis JE. RI photometry of 2MASS-selected late M and L dwarfs. Publ Astron Soc Pac. 2006; 118:659–670.
12. Costa E, et al. The solar neighbourhood. XVI. Parallaxes from CTIOPI: final results from the 1.5m telescope program. Astron J. 2006; 132:1234–1247.
13. Filippazzo JC, et al. Fundamental parameters and spectral energy distributions of young and field age objects with masses spanning the stellar to planetary regime. Astrophys J. 2015; 810:158.
14. Gillon M, et al. The TRAPPIST survey of southern transiting planets. I. Thirty eclipses of the ultra-short period planet WASP-43 b. Astron & Astrophys. 2012; 524:A4.
15. Reiners A, Basri G. A volume-limited sample of 63 M7-M9.5 dwarfs. II. Activity, magnetism, and the fade of the rotation-dominated dynamo. Astrophys J. 2010; 710:924–935.
16. Hosey AD, et al. The solar neighbourhood. XXXVI. The long-term photometric variability of nearby red dwarfs in the VRI optical bands. Astron J. 2015; 150:6.
17. Liang Y, et al. Tests of the planetary hypothesis for PTFO8-8695b. Astrophys J. 2015; 812:48.
18. Stelzer B, Marino A, Micela G, López-Santiago J, Liefke C. The UV and X-ray activity of the M dwarfs within 10 pc of the Sun. Mon Not R Astron Soc. 2013; 431:2063–2079.
19. Lopez ED, Fortney JJ, Miller N. How thermal evolution and mass-loss sculpt populations of super-Earths and subNeptunes: Application to the Kepler-11 system and beyond. Astrophys J. 2012; 761:59.
20. Rogers LA. Most 1.6 Earth-radius planets are not rocky. Astrophys J. 2015; 801:41.
21. Wolfgang A, Lopez E. How rocky are they? The composition distribution of Kepler's sub-Neptune planet candidates within 0.15 AU. Astrophys J. 2015; 806:183.
22. Seager S, Kuchner M, Hier-Majumder CA, Militzer B. Mass-radius relationships for solid exoplanets. Astrophys J. 2007; 669:1279–1297.
23. Holman MJ, Murray NW. The use of transit timing to detect terrestrial-mass extrasolar planets. Science. 2005; 307:1288–1291. [PubMed: 15731449]
24. De Wit J, Seager S. Constraining exoplanet mass from transmission spectroscopy. Science. 2013; 342:1473–1477. [PubMed: 24357312]
25. Kasting JF, Whitmire DP, Reynolds RT. Habitable zones around main-sequence stars. Icar. 1993; 101:108–128.
26. Leconte J, et al. 3D climate modelling of close-in land planets: Circulation patterns, climate moist instability, and habitability. Astron & Astrophys. 2013; 554:A69.
27. Menou K. Water-trapped world. Astrophys J. 2013; 774:51.
28. Driscoll PE, Barnes R. Tidal heating of Earth-like exoplanets around M stars: thermal, magnetic, and orbital evolutions. Astrobio. 2015; 15:739–760.
29. France K, et al. The ultraviolet radiation environment around M dwarf exoplanet host stars. Astrophys J. 2013; 763:149.
30. Tiang F, Ida S. Water contents of Earth-mass planets around M-dwarfs. Nature Geoscience. 2015; 8:177–180.
31. Gizis JE, et al. New neighbours from 2MASS: activity and kinematics at the bottom of the main sequence. Astron J. 2000; 120:1085–1099.
32. Bartlett JL. Knowing our neighbours: Fundamental properties of nearby stars. Publ Astron Soc Pac. 2007; 119:828–829.
33. Schmidt SJ, Cruz KL, Bongiorno BJ, Liebert J, Reid IN. Activity and kinematics of ultracool dwarfs, including an amazing flare observation. Astron J. 2007; 133:2258–2273.
34. Lee K-G, Berger E, Knapp GR. Short-term Hα variability in M dwarfs. Astrophys J. 2010; 708:1482–1491.
35. Rayner JT, et al. SpeX: A Medium-Resolution 0.8-5.5 Micron Spectrograph and Imager for the NASA Infrared Telesce. Publ Astron Soc Pac. 2003; 115:362–382.
36. Reiners A, Basri G. A volume-limited sample of 63 M7-M9.5 dwarfs. I. Space motion, kinematics age, and lithium. Astrophys J. 2009; 705:1416–1424.
37. Vacca WD, Cushing MC, Rayner JT. A Method of Correcting Near-Infrared Spectra for Telluric Absorption. Publ Astron Soc Pac. 2003; 115:389–409.

Europe PMC Funders Author Manuscripts

38. Cushing MC, Vacca WD, Rayner JT. Spextool: a spectral extraction package for SpeX, a 0.8-5.5 micron cross-dispersed spectrograph. Publ Astron Soc Pac. 2004; 116:362–376.
39. Rojas-Ayala B, Covey KR, Muirhead PS, Lloyd JP. Metallicity and temperature indicators in M dwarf K-band spectra: testing new and updated calibrations with observations of 133 solar neighbourhood M dwarfs. Astrophys J. 2012; 748:93.
40. Mann AW, et al. Prospecting in ultracool dwarfs: measuring the metallicities of mid- and late-M dwarfs. Astron J. 2014; 147:160.
41. Skrutskie MF, Meyer MR, Whalen D, Hamilton C. The two micron all sky survey (2MASS). Astron J. 2006; 131:1163–1183.
42. Cutri, RM., et al. Vizier Online Data Catalog II/311: WISE all-sky data release. 2012. http://vizier.cfa.harvard.edu/viz-bin/VizieR?-source=II/311
43. Cruz KL, et al. Meeting the cool neighbours. IX. The luminosity function of M7-L8 ultracool dwarfs in the field. Astron J. 2007; 133:439–467.
44. Baraffe I, Homeier D, Allard F, Chabrier G. New evolutionary models for pre-main sequence and main sequence low-mass stars down to the hydrogen-burning limit. Astron & Astrophys. 2015; 577:A42.
45. Siegler N, Close LM, Mamajeck EE, Freed M. An adaptive optics survey of M6.0-M7.5 stars: discovery of three very low mass binary system including two probable Hyades member. Astrophys J. 2003; 598:1265–1276.
46. Siegler N, Close LM, Cruz KL, Martín EL, Reid IN. Discovery of two very low mass binaries: final results of an adaptive optics survey of nearby M6.0-M7.5 stars. Astrophys J. 2005; 621:1023–1032.
47. Janson M, et al. The AstraLux large M-dwarf multiplicity survey. Astrophys J. 2012; 754:44.
48. Bouy H, et al. Multiplicity of nearby free-floating ultracool dwarfs: a Hubble Space Telescope WFPC2 search for companions. Astron J. 2003; 126:1526–1554.
49. Barnes JR, et al. Precision radial velocities of 15 M5-M9 dwarfs. Mon Not R Astron Soc. 2014; 439:3094–3113.
50. Tanner A, et al. Keck NIRSPEC radial velocity observations of late M-dwarfs. Astrophys J. 2012; 203(Suppl):10.
51. Burgasser AJ, et al. WISE J072003.20-084651.2: and old and active M9.5 + 75 spectral binary 6 pc from the Sun. Astron J. 2015; 149:104.
52. Zacharias N, et al. The second US Naval Observatory CCD astrograph catalog (UCAC2). Astron J. 2004; 127:3043–3059.
53. Izmailov IS, et al. Astrometric CCD observations of visual double stars at the Pulkovo Observatory. Astron L. 2010; 36:349–354.
54. Minkowski, RL., Abell, GO. The National Geographic Society-Palomar Observatory Sky Survey. Basic Astronomical Data: Stars and stellar systems. Strand, KA., editor. University of Chicago Press; Chicago, IL USA: 1963. p. 481-487.
55. Jehin E, et al. TRAPPIST: TRAnsiting Planets and PlanetesImals Small Telescope. Msngr. 2011; 145:2–6.
56. Stetson PB. DAOPHOT - A computer program for crowded-field stellar photometry. Publ Astro Soc Pacific. 1987; 99:191–222.
57. Indian Institute of Astrophysics. Indian Astronomical Observatory, Hanle. 2m Telescope - Hanle Faint Object Spectrograph Camera. 2011. http://www.iiap.res.in/iao_hfosc
58. Pirard J-F, et al. HAWK-I: A new wide-field 1- to 2.5 μm imager for the VLT. Proc SPIE. 2004; 5492:1763–1772. DOI: 10.1117/12.578293
59. Casali, M., et al. The UKIRT IR Wide-Field Camera (WFCAM). In: Clowes, R.Adamson, A., Bromage, G., editors. The new era of of wide-field astronomy, ASPC Conference Series Vol. 232; 2001. p. 357-363.
60. Eastman J, Siverd R, Gaudi BS. Achieving Better Than 1 Minute Accuracy in the Heliocentric and Barycentric Julian Dates. Publ Astro Soc Pacific. 2010; 122:935–946.
61. Mandel K, Agol E. Analytic light curves for planetary transit searches. Astrophys J. 2002; 580:L171–L175.

62. Schwarz G. Estimating the dimension of a model. Ann Statist. 1978; 6:461–464.
63. Claret A, Bloemen S. Gravity and limb-darkening coefficients for the Kepler, CoRoT, Spitzer, uvby, UBVRIJHK, and Sloan photometric systems. Astron & Astrophys. 2011; 529:A75.
64. Gelman A, Rubin DB. Inference from Iterative Simulation Using Multiple Sequences. Statist Sciences. 1992; 7:457–472.
65. Winn, JN. Exoplanets transits and occultations. Exoplanets. Seager, S., editor. University of Arizona Press Tucson; AZ USA: 2010.
66. Agol E, Steffen J, Sari R, Clarkson W. On detecting terrestrial planets with timing of giant planet transits. Mon Not R Astron Soc. 2005; 359:567–579.
67. Davenport JRA, et al. Kepler flares II: the temporal morphology of white-light flares on GJ1243. Astrophys J. 2014; 797:122.
68. Scargle JD. Studies in astronomical time series analysis. II - Statistical aspects of spectral analysis of unevenly spaced data. Astrophys J. 1982; 263:835–853.
69. Goldreich P, Soter S. Q in the solar system. Icarus. 1966; 5:375–389.
70. Murray, CD., Dermott, SF. Solar System Dynamics. Cambridge University Press; Cambridge, UK: 2001.
71. Limbach MA, Turner EL. The orbital eccentricity - multiplicity relation and the solar system. Proc Nat Ac Sci. 2015; 112:20–24.
72. Chambers JE. A hybrid symplectic integrator that permits close encounters between massive bodies. Mon Not R Astron Soc. 1999; 304:793–799.
73. Charbonneau D, et al. A super-Earth transiting a nearby low-mass star. Nature. 2009; 462:891–894. [PubMed: 20016595]
74. Miller-Ricci E, Seager S, Sasselov D. The atmospheric signatures of super-Earths: how to distinguish between hydrogen-rich and hydrogen-poor atmospheres. Astrophys J. 2009; 690:1056–1067.
75. Han E, et al. The exoplanet orbit database. II. Updates to exoplanet.org. Publ Astro Soc Pacific. 2014; 126:827–837.
76. Kreidberg L, et al. Clouds in the atmosphere of the super-Earth exoplanet GJ1214b. Nature. 2014; 505:69–72. [PubMed: 24380954]
77. Berta ZK, et al. The flat transmission spectrum of the super-Earth GJ1214b from Wide Field Camera 3 on the Hubble Space Telescope. Astrophys J. 2012; 747:35.
78. Snellen IAG, de Kock RJ, de Mooij EJW, Albrecht S. The orbital motion, absolute mass and high-altitude winds of exoplanet HD209458b. Nature. 2010; 465:1049–1051. [PubMed: 20577209]
79. Rodler F, López-Morales M. Feasibility studies for the detection of O_2 in an Earth-like exoplanet. Astrophys J. 2014; 781:54.

Europe PMC Funders Author Manuscripts

Europe PMC Funders Author Manuscripts

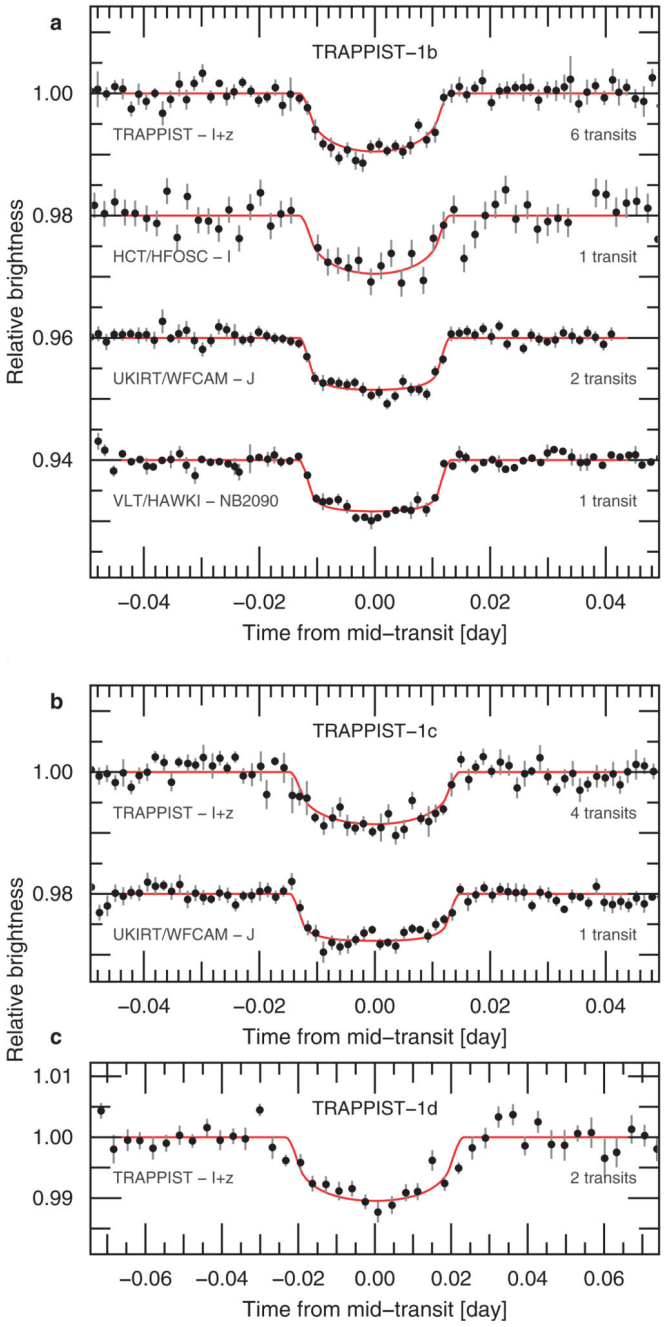

Figure 1. Transit photometry of the TRAPPIST-1 planets.

Each light curve is phased to the time of inferior conjunction (mid-transit time) of the object. The light curves are binned by 2-minute intervals for planet b (**a**) and 5-minute interval for planet c (**b**) and d (**c**). The best-fit transit models as derived from the global analysis of the data are overplotted on the light curves (red lines). The light curves are shifted along the *y*-axis for the sake of clarity. For the HCT/HFOSC light curve, the data are unbinned and the error bars are the formal measurement errors. For the other light curves, the error bars are the standard errors of the mean of the measurements in the bin.

Europe PMC Funders Author Manuscripts

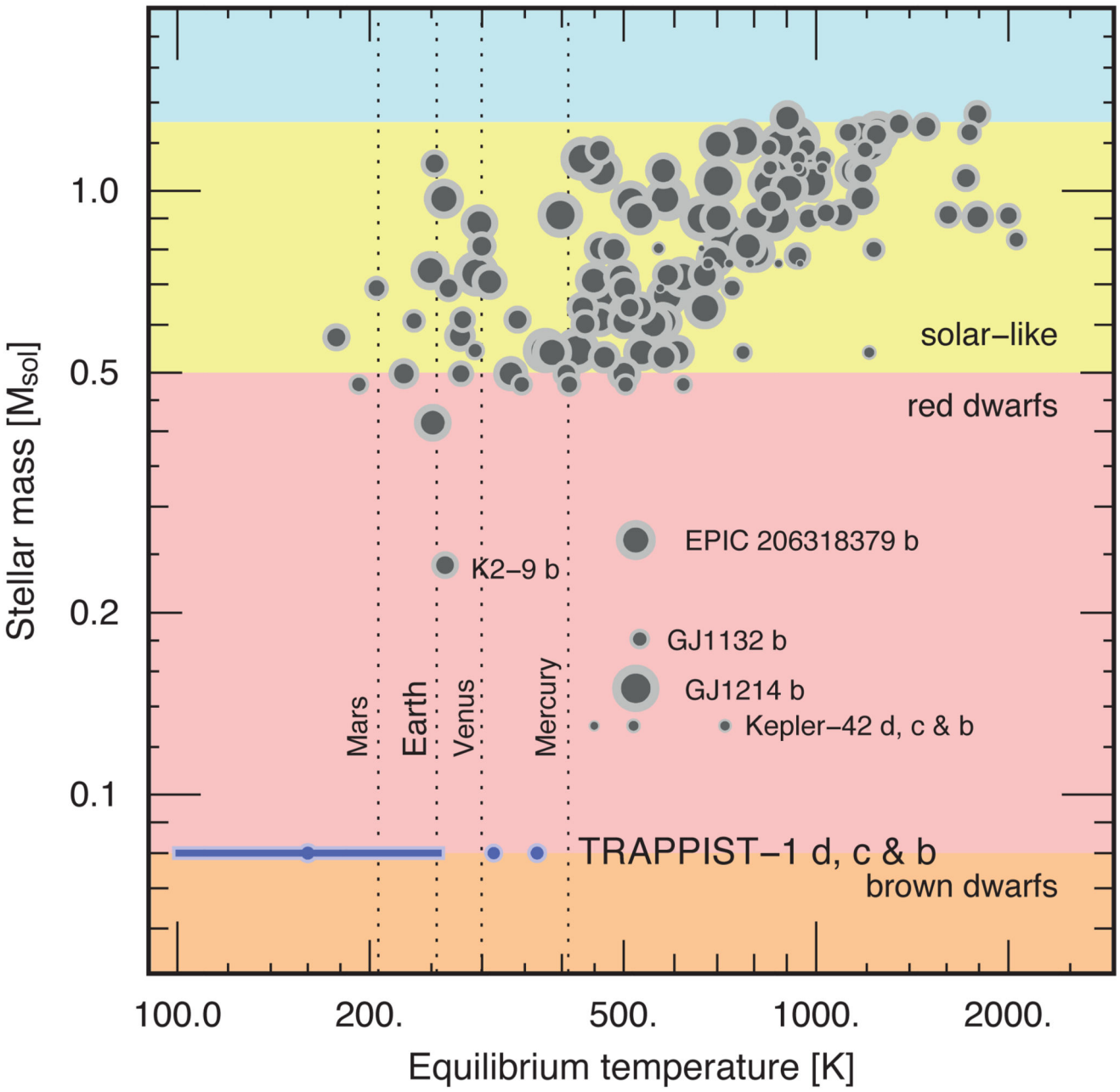

Figure 2. Host star masses and temperatures of the known sub-Neptune-size exoplanets.

The size of the symbols linearly scales with planet radius. The background is color-coded as a function of stellar mass (in units of the Sun's mass). TRAPPIST-1 is at the boundary between hydrogen burning stars and brown dwarfs. Equilibrium temperatures are estimated neglecting atmospheric effects and assuming an Earth-like albedo of 0.3. The positions of the solar system terrestrial planets are given with dotted lines for reference. The range of possible equilibrium temperatures of TRAPPIST-1d is represented by a solid bar. The location of the dot is the most likely solution. Only the exoplanets with a measured radius equal to or smaller than GJ1214b's are included in the figure.

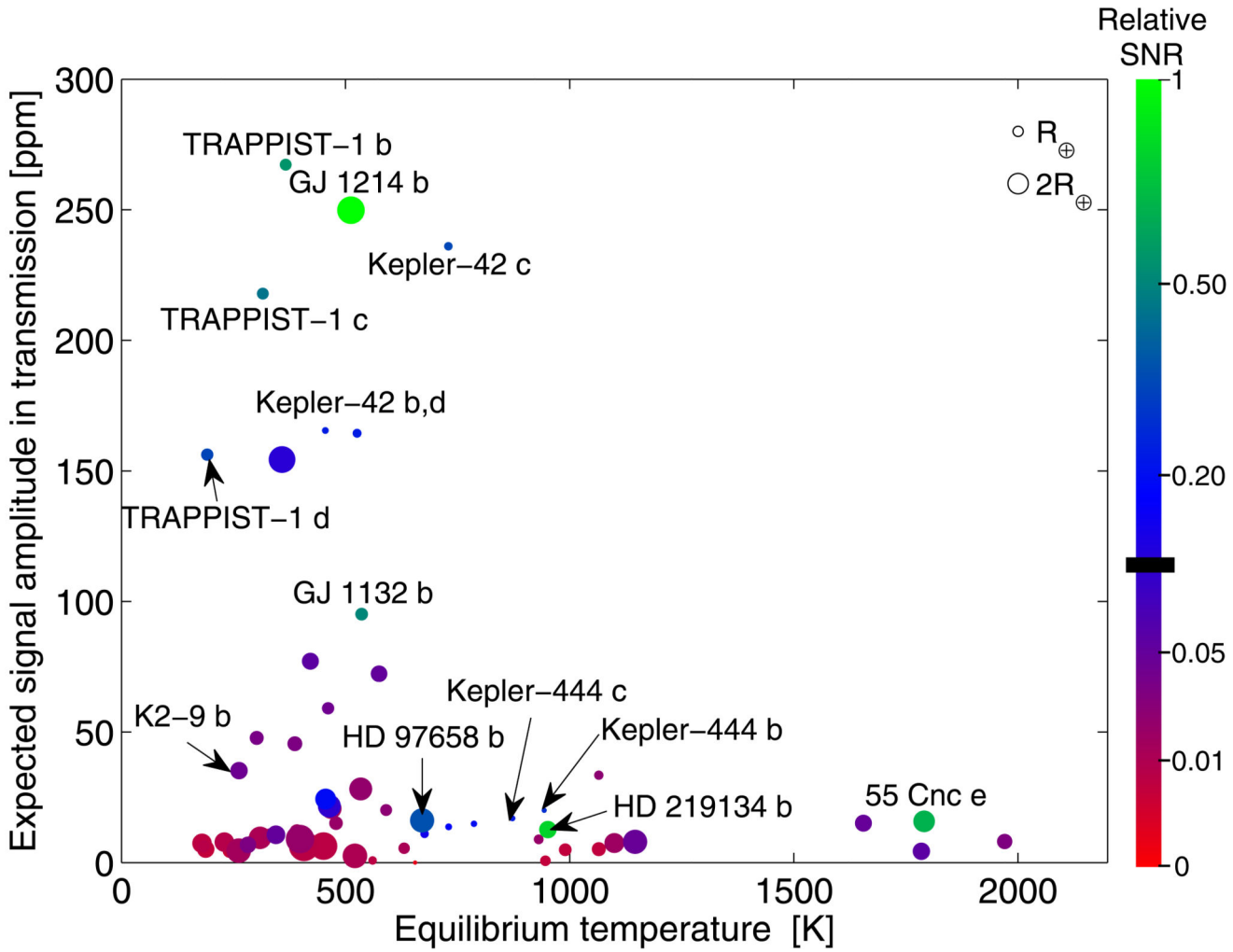

Figure 3. Potential for atmospheric characterization of known transiting sub-Neptune-size exoplanets.

Estimation of the signal in transmission (in ppm, parts per million and for clear water-dominated atmospheres with mean molecular weight μ = 19) and signal-to-noise (SNR) in transmission (normalized to GJ1214b's) versus equilibrium temperatures (T_{eq}) assuming a Bond albedo of 0.3. The black line indicates the SNR ratio requiring 200(500)[1000] hrs of in-transit observations with JWST to yield a planet's atmospheric temperature with a relative uncertainty below 15% and abundances within a factor of 4 in the case of a $H_2O(N_2)[CO_2]$-dominated atmosphere (μ=19(28)[39]). Only the exoplanets with a measured radius equal to or smaller than GJ1214b's are included in the figure. The size of the circular symbol of each planet is proportional to its physical size.

Europe PMC Funders Author Manuscripts

Table 1
Properties of the TRAPPIST-1 planetary system

Parameter	Value		
Star	**TRAPPIST-1 = 2MASS J23062928-0502285**		
Magnitudes	V=18.80±0.08, R=16.47±0.07, I=14.0±0.1, J=11.35±0.02, K=10.30±0.02		
Distance $d_\star$	12.1±0.4 parsecs12		
Luminosity $L_\star$	0.000525±0.000036 $L_\odot$13		
Mass $M_\star$	0.080±0.009 $M_\odot$		
Radius $R_\star$	0.117±0.004 $R_\odot$		
Density $\rho_\star$	$50.3^{+5.7}_{-3.3}$ $\rho_\odot$		
Effective temperature T_{eff}	2550±55 K		
Metallicity [Fe/H]	+0.04±0.08 (from near-IR spectroscopy)		
Rotation period P_{rot}	1.40±0.05d (from TRAPPIST photometry)		
Age $\tau_\star$	>500 Myr13		
Planets	**TRAPPIST-1b**	**TRAPPIST-1c**	**TRAPPIST-1d**
Orbital period P	1.510848 ±0.000019d	2.421848 ±0.000028d	{4.551, 5.200, 8.090, 9.101, 10.401, 12.135, 14.561, **18.202**, 24.270, 36.408, 72.820}d[a]
Mid-transit time t_0-2,450,000 [BJD_{TDB}]	7322.51765 ±0.00025	7362.80520 ±0.00033	7294.7744 ±0.0015[b]
Transit depth $(R_p/R_\star)^2$	0.754±0.025 %	0.672±0.042 %	0.826±0.073%[b]
Transit impact parameter b	0.21±0.14 $R_\star$	0.25±0.15 $R_\star$	0.20±0.15 $R_\star$[b]
Transit duration W	36.12±0.46 min	41.78±0.81 min	83.3±2.5 min [b]
Orbital inclination i	89.41±0.41 deg	89.50±0.31 deg	89.90±0.10 deg[b]
Orbital eccentricity e	0 (fixed)	0 (fixed)	0 (fixed)
Radius R_p	1.113±0.044 R_{Earth}	1.049±0.050 R_{Earth}	1.163±0.065 R_{Earth}[b]
Scale parameter $a/R_\star$	$20.45^{+0.43}_{-0.81}$	$28.0^{+0.6}_{-1.1}$	{41:271}[c]
Semi-major axis a	0.01111 ±000040 au	0.01522 ±0.00055 au	{0.022:0.146}[c] au
Irradiation S_p	4.25±0.38 S_{Earth}	2.26±0.21 S_{Earth}	{0.02:1.0}[c] S_{Earth}
Equilibrium temperature T_{eq}			
with Bond albedo of 0.00	400±9 K	342±8 K	{110:280}[c] K
with Bond albedo of 0.75	285±7 K	242±6 K	{75:200}[c] K

The values and 1-sigma errors given for the planetary parameters and for the stellar mass, radius, density, and effective temperature were deduced from a global analysis of the photometric data, including *a priori* knowledge on the stellar properties (see Methods).

[a]These are the potential orbital periods of TRAPPIST-1d based on non-continuous observations.

[b]Assuming P=18.20175±0.00045d, the most likely values for the period as derived from the shape of the transits.

[c]Range allowed by the set of possible periods.